



**HAL**  
open science

## About Schlunder's model: A numerical study of evaporation from partially wet surfaces

Marouane Talbi, Marc Prat

► **To cite this version:**

Marouane Talbi, Marc Prat. About Schlunder's model: A numerical study of evaporation from partially wet surfaces. *Drying Technology*, 2018, 37, pp.513-524. 10.1080/07373937.2018.1506929 . hal-02355914

**HAL Id: hal-02355914**

**<https://hal.science/hal-02355914>**

Submitted on 8 Nov 2019

**HAL** is a multi-disciplinary open access archive for the deposit and dissemination of scientific research documents, whether they are published or not. The documents may come from teaching and research institutions in France or abroad, or from public or private research centers.

L'archive ouverte pluridisciplinaire **HAL**, est destinée au dépôt et à la diffusion de documents scientifiques de niveau recherche, publiés ou non, émanant des établissements d'enseignement et de recherche français ou étrangers, des laboratoires publics ou privés.



## Open Archive Toulouse Archive Ouverte (OATAO)

OATAO is an open access repository that collects the work of Toulouse researchers and makes it freely available over the web where possible

This is an author's version published in: <http://oatao.univ-toulouse.fr/24632>

**Official URL:** <https://doi.org/10.1080/07373937.2018.1506929>

**To cite this version:**

Talbi, Marouane  and Prat, Marc  *About Schlunder's model: A numerical study of evaporation from partially wet surfaces.* (2018) *Drying Technology*, 37. 513-524. ISSN 0737-3937

Any correspondence concerning this service should be sent to the repository administrator: [tech-oatao@listes-diff.inp-toulouse.fr](mailto:tech-oatao@listes-diff.inp-toulouse.fr)

# About Schlünder's model: A numerical study of evaporation from partially wet surfaces

M. Talbi and M. Prat

Institut de Mécanique des Fluides de Toulouse, IMFT, Université de Toulouse, CNRS, Toulouse, France

## ABSTRACT

Estimate of evaporation rate from a partially wet surface using Schlünder's analytical model is assessed from comparison with numerical simulations. The influence of pore shape and pore size heterogeneity is explored as well as the limit of the very low wet surface fractions. A modified form of Schlünder's formula is proposed for the heterogeneous surfaces by using the pore influence surface areas obtained from a minimum distance surface tessellation technique. The modified formula provides a simple method for coupling the external transfer and the internal transfer in the pore network modeling of drying.

## KEYWORDS

External transfer; heterogeneous porous surface; pore network; porous media

## Introduction

One of the most puzzling aspects of drying of porous media is the possible existence of a long constant rate period (CRP), namely a period over which the evaporation rate varies little whereas the water content varies appreciably. Since drying is a phenomenon coupling internal transfers, that is, inside the porous media, and external transfers, that is, in the gas phase at the evaporative surface of the porous medium, both types of transfer should play a role in the existence and duration of the CRP. Qualitatively, the CRP is "explained" from an internal transfer standpoint by the fact that capillary effects can maintain the surface sufficiently wet. This can also be viewed as a consequence of the capillary pumping effect (see below). It is now well known that drying of porous media can be analyzed within the realm of two-phase flow theory in porous media<sup>[1]</sup> as an invasion percolation process.<sup>[2-4]</sup> This means that the bigger pores are first invaded whereas smaller pores stay wet at the surface. For a meniscus to stay at the entrance of a smaller pore at the surface, a liquid flow in this pore should equilibrate the evaporation rate from this pore. This is the capillary pumping effect, that is, a net flow from the inside of the medium toward the smaller pores at the surface. However, since bigger pores are invaded, the density of wet pores (fraction of the pores at the

surface with a pinned meniscus) decreases during the CRP. In other terms, the surface is less and less wet but this does not change appreciably the evaporation rate, at least as long the surface wet fraction is high enough. Then we have to explain why the evaporation rate from a partially wet surface can remain approximately unchanged whereas the surface becomes less and less wet. This is essentially the point studied by Schlünder.<sup>[5,6]</sup> Extending the work of Suzuki and Maeda,<sup>[7]</sup> Schlünder essentially showed that the evaporation rate from a surface covered by discrete wet spots is essentially the same as the evaporation rate from the same surface totally wet provided that the wet spots are evenly distributed over the surface and their diameter is small compared to the typical thickness of the external mass transfer layer. This result was obtained assuming that the external mass transfer is governed by diffusion, at least in a small layer adjacent to the surface (the viscous sub-layer in the analysis of Schlünder), for example, Haghghi et al.<sup>[8]</sup> The analytical relationship proposed by Schlünder reads

$$\frac{J}{J_{\text{ref}}} = \frac{1}{1 + \frac{2r_p}{\pi\delta} \sqrt{\frac{\pi}{4\theta}} \left[ \sqrt{\frac{\pi}{4\theta}} - 1 \right]}, \quad (1)$$

where  $J$  is the evaporation rate,  $\delta$  is the thickness of the diffusive layer adjacent to the surface,  $r_p$  is the radius of the wet spots (pores) at the surface.  $\theta = \frac{\pi r_p^2}{a^2}$  is the

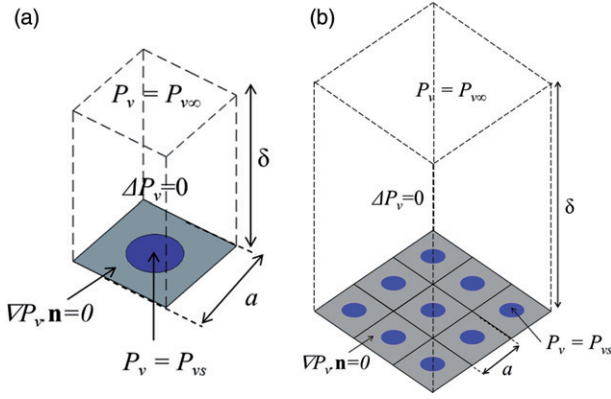


**Figure 1.** Computational domains: (a) single unit cell and (b)  $3 \times 3$  square arrangement of wet surface pores.

wetted fraction of the surface where  $a$  is the size of a square unit cell with a circular pore opening in its center (see Figure 1(a)). The length  $a$  can also be interpreted as the mean distance between the pores at the surface. In Equation (1),  $J_{\text{ref}}$  is the evaporation rate when the surface is entirely covered by liquid,

$$J_{\text{ref}} = \frac{M_v}{RT} D a^2 \frac{(P_{vs} - P_{v\infty})}{\delta}, \quad (2)$$

where  $M_v$ ,  $R$ , and  $T$  are the water molecular weight, the universal gas constant, and the temperature.  $D$  is the molecular diffusion coefficient of vapor in the binary mixture formed by air and the vapor.  $P_{vs}$  and  $P_{v\infty}$  are the vapor pressure at the pore surface (saturated vapor pressure) and in the external gas at the distance  $\delta$  from the porous surface, respectively.

Hence Equation (1) provides an explicit relationship between the evaporation rate and the degree of occupancy of the porous surface by the liquid.

Schlünder's relationship thus analyzes the CRP from a pure external mass transfer standpoint. However, as discussed in Moghaddam et al. and Lehmann and Or,<sup>[9,10]</sup> drying is less simple than considered in Schlünder's analysis. For instance, the pore sizes are not uniform at the surface and vary from one pore to another. The impact of this variability must be assessed. Nevertheless, Schlünder's relationship is still today the only analytical expression linking the evaporation rate to the degree of occupancy of the surface by the liquid. Since the evaporation rate decreases according to Equation (1) when  $\theta$  is sufficiently small, Equation (1) was also used later by Schlünder<sup>[11]</sup> to explain the end of the CRP and thus the transition toward the falling rate period (FRP), another key issue in the drying theory.

Since drying is essentially a coupled problem between the transfer inside the porous medium and in the external gas domain with which the porous

medium is in contact on one or several sides, the correct modeling of the coupling is crucial. In the simpler approach, the mass transfer at the surface is modeled using a mass transfer coefficient, for example, Chen and Pei.<sup>[11]</sup> Thus in the case, the equations governing the mass transfer in the external gas are not solved explicitly all along the drying process. The problem with this approach is that the variation of the mass transfer coefficient during the drying process is not known. Therefore this approach is rarely truly predictive. A more satisfactory approach consists in solving together the equations governing the transfer in the external gas and inside the porous medium. Such an approach when the transfers inside the porous medium are modeled using the continuum approach to porous media can be found, for example, in the references.<sup>[12-17]</sup> A somewhat similar coupling strategy has also been developed in relation with the pore network modeling (PNM) of drying, for example, Xu and Pillai.<sup>[18]</sup> Although the general approach involving to solve the Navier–Stokes equations together with the vapor transport equation is certainly the most versatile in relation with drying problems, simplified versions can also be useful, for instance in order to perform comparisons with laboratory experiments, for example, Veran and Prat.<sup>[19]</sup> Such a simple case is when the external mass transfer is essentially driven by diffusion, a situation thus similar to the situation considered by Schlünder. One can thus wonder whether Schlünder's formula or a variant of Schlünder's formula could be useful in relation with the PNM of drying. In this respect, it should be noted that the results presented in Moghaddam et al.<sup>[9]</sup> as well as in previous works using a pore network model, for example, Yiotis et al.,<sup>[20]</sup> were based on simulations using a quite coarse grid in the external mass transfer boundary layer. Clearly, this aspect of PNM needs improvement.

To sum up, the objectives of the present paper are triple: (1) assessing Schlünder's relationship for a greater variety of wet pore shapes than in previous works, (2) looking at the asymptotic case where the wet spots are far apart from each other, and (3) adapting Schlünder's formula to the case of heterogeneous surface for application to the PNM simulations of drying.

## Method

The study is based on numerical solutions of the diffusion equation governing the vapor concentration in the external mass transfer boundary layer. As depicted

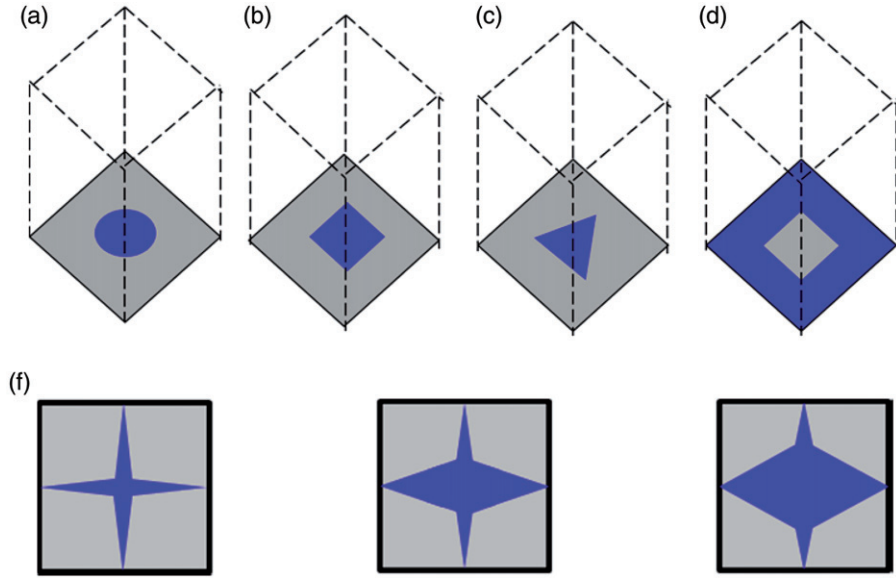


**Figure 2.** The various surface elementary pore shapes (wet zone in blue, solid surface in grey): (a) circular, (b) square, (c) triangle, (d) square complement, and (e) Star shapes corresponding to  $\theta = 0.1$ ,  $\theta = 0.2$ , and  $\theta = 0.3$ , respectively.

in [Figure 1](#), the computational domain  $\Omega$  is a parallelepiped domain with the partially wet surface localized at its bottom. Using the vapor partial pressure  $P_v$  as main variable, the problem to be solved in  $\Omega$  reads

$$\Delta P_v = 0, \quad (3)$$

where  $\Delta$  is here the Laplacian (Laplace operator). [Equation \(3\)](#) thus corresponds to the steady-state diffusion equation when the temperature variations can be ignored and the diffusion coefficient is constant. On the lateral boundaries, a zero flux condition is imposed ( $\nabla P_v \cdot \mathbf{n} = 0$ , where  $\mathbf{n}$  is the unit normal vector at the considered surface). On the top surface, the vapor partial pressure is known,

$$P_v = P_{v\infty} \text{ at } z = \delta \quad (4)$$

On the partially wet surface  $\partial\Omega_b$  (bottom surface at  $z=0$ ), the vapor partial pressure is known on the wet regions, that is

$$P_v = P_{vs} \text{ at } z = 0 \text{ on } \partial\Omega_{bw}, \quad (5)$$

where  $P_{vs}$  is the saturated vapor pressure at the considered temperature (the temperature is uniform all over the computational domain). On the solid part of  $\partial\Omega_b$ , a zero flux condition is imposed

$$\nabla P_v \cdot \mathbf{n} = 0 \text{ at } z = 0 \text{ on } \partial\Omega_{bs}. \quad (6)$$

[Equations \(3\)–\(6\)](#) are solved using the simulation software COMSOL Multiphysics. Once the vapor pressure field has been computed the evaporation rate is computed as

$$J = \int_{\partial\Omega_{bw}} \left( -D \frac{M_v}{RT} \nabla P_v \cdot \mathbf{n} \right) d\Omega \text{ at } z = 0. \quad (7)$$

In typical drying experiments,  $\delta$  is on the order of 1 mm while a typical mean distance between pores is of the order of 100  $\mu\text{m}$  or less. Thus, unless otherwise mentioned, all the simulations presented in what follows have been performed for  $\delta = 1 \text{ mm}$  and  $a = 100 \mu\text{m}$ . However, it can be noted that what matters is actually the ratio  $\delta/a$ . Thus, the presented results directly apply to other values of  $a$  or  $\delta$  as long as  $\delta/a = 10$ .

### Influence of pore shape

To derive his formula, Schlünder has actually considered a system of hemispherical droplets. Assuming a square arrangement of the droplets, he actually considered a single unit cell of parallelepiped shape with a droplet lying in the middle of the bottom surface of the parallelepiped domain. Since pores are not hemispherical droplets, it is interesting to examine the impact of the pore shape. Circular pores are obvious candidates but it is clear that the pore shape is often quite different from a circular tube. For this reason, we have also tested other elementary shapes such as square, triangle, and star shapes. The various tested shapes are depicted in [Figure 2](#) while a comparison between the results obtained using Schlünder's relationship and the results obtained numerically for the different shapes is presented in [Figure 3](#).

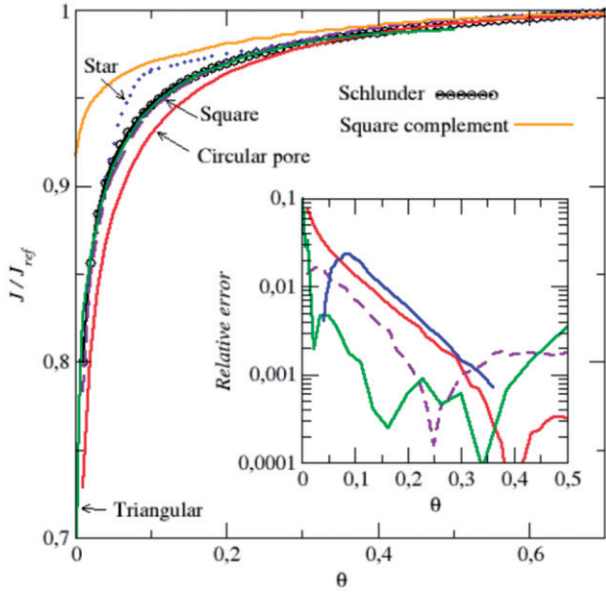


**Figure 3.** Test of Schlünder's relationship (Eq. (1)) for the various pore shapes.  $\delta = 1$  mm,  $a = 0.1$  mm (the dashed purple line corresponds to the square shape and the green solid line to the triangular shape). The inset shows the relative error between the numerical results and Schlünder's formula (same color code as for the main plot, the error for the square complement is not plotted).

To perform this comparison we keep  $\delta = 1$  mm and  $a = 100 \mu\text{m}$  and vary the wet surface area  $S_w$  for the various shapes. Thus,  $\theta = \frac{S_w}{a^2}$ . To use Equation (1), we also need to specify the pore radius  $r_p$ . For shapes different from the circular shape, we define  $r_p$  as the circular pore radius having the same wetted area as the considered shape. Hence  $r_p$  is determined from the relationship  $\pi r_p^2 \approx S_w$ .

As can be seen from Figure 3, the variation of the evaporation rate with  $\theta$  is sensitive to the pore shape. Somewhat surprisingly in view of the analytical method used by Schlünder to derive his formula, the numerical results for the circular pore lead to lower evaporation rates compared to the estimate with Schlünder's formula. It is important to mention here that very refined meshes were used to obtain the results shown in Figure 3. So the discrepancy cannot be attributed to a lack of mesh refinement. It is attributed to the approximation made by Schlünder in deriving his formula. However, the agreement with Schlünder's formula is excellent for the square and triangle pore shapes. The star shape leads to a greater discrepancy, at least for  $\theta$  around 0.1. Note that the star shape is anisotropic (see Figure 2(f)) and it is the shape which is obviously the less closer to a circular shape among the considered shapes. As shown in the inset in Figure 3, the relative error  $|J_{\text{num.}} - J_{\text{Schl.}}|/J_{\text{Schl.}}$

is, however, reasonably low for all shapes, that is, less than 10% and actually on the order of a few percent only, except with the circular and triangle shapes for  $\theta < 0.05$ . The case of the very low  $\theta$  is examined in more details after the next section, which briefly presents the results obtained for the case of the square complement (Figure 2(d)).

### A counter – example

Since Schlünder's formula was derived considering a spatially periodic square arrangement of droplets, it can be expected that it leads to much less good results when the distribution of the liquid at the surface is markedly different from an even distribution of isolated wet spots.

Consider, for example, the situation where the central region of the unit cell corresponds to a solid surface (no flux) whereas the complementary surface is wet (the case of square unit cell is illustrated in Figure 2(d)). The comparison between the simulations and the predictions using Schlünder's formula for this case is depicted in Figure 3 (compare the orange line with the black line with empty circles).

As can be seen, using Schlünder's formula is not a good idea for this case. In summary, as illustrated with this example as well as with the star shape if the wet region shape in the unit cell is too different from a circular pore, Schlünder's formula is not reliable. Of course, it can be noted that this essentially holds when Schlünder's formula indicates a noticeable impact of  $\theta$  on the evaporation rate, that is, when  $\theta$  is sufficiently low ( $\theta < 0.3$  in Figure 3).

### Evaporation rate for very low wetted surface fractions

The motivation for studying the evaporation rate when the wetted surface fraction is very low comes from the study of saline evaporation from porous media, for example, Eloukabi et al.<sup>[21]</sup> When a salt crust forms at the surface, it is often observed that the evaporation rate is severely reduced compared to the situation for pure water. The evaporation rate can be reduced by at least one order of magnitude. One simple option to explain this very low evaporation rate is to consider that the crust is still wet but with a quite low density of active pores at its surface (due to pore clogging by the precipitation of the salt). Active pores mean wet pores where evaporation takes place. Thus, we are interested here in Schlünder's relationship when  $\theta \ll 1$ . In this limit, Equation (1) can be written

as

$$\frac{J}{J_{\text{ref}}} = \frac{1}{1 + 0.5 \frac{r_p}{\theta \delta}} \approx \frac{2\theta \delta}{r_p} \approx 2\sqrt{\pi} \theta \frac{\delta}{a} \approx 2\pi \frac{r_p \delta}{a^2}. \quad (8)$$

Thus, Schlünder's relationship suggests that the evaporation rate should vary with the square root of wetted surface fraction  $\theta$  when  $\theta \ll 1$ . Using Equation (2), the evaporation rate from a surface element of size  $a$  is given in this very low wetted surface fraction limit by

$$J \approx \frac{2\theta M_v}{r_p RT} Da^2 (P_{vs} - P_{v\infty}) = 2\pi r_p \frac{M_v}{RT} D (P_{vs} - P_{v\infty}). \quad (9)$$

As it could be expected, Equation (9) is almost identical to the expression giving the evaporation rate of a single flat droplet (a disk) on a flat plate in an infinite half-space, for example, Picknett and Bexon<sup>[22]</sup> and Hu and Larson.<sup>[23]</sup> The difference only lies in the numerical factor  $2\pi$  in Equation (9) versus 4 for the isolated droplet expression.<sup>[22,23]</sup> As indicated by Equation (9), a key characteristic of diffusive evaporation is that the evaporation rate is proportional to the perimeter of the droplet and not to its surface area. The difference in the prefactor is not surprising since the conditions considered by the different authors to derive their analytical expression are different. Whereas Schlünder considered the evaporation from a half sphere in a spatially periodic system, Picknett and Bexon<sup>[22]</sup> and Hu and Larson<sup>[23]</sup> considered the somewhat simpler case of a single droplet in an infinite half-space.

In order to evaluate the applicability of Equation (8), we have computed the evaporation rate for the situation depicted in Figure 1(a) for  $\theta$  varying in the range  $[10^{-6} - 10^{-3}]$  (which corresponds to  $r_p/a$  varying between  $5.64 \times 10^{-4}$  and 0.0178 for a circular pore). The results are shown in Figure 4.

As can be seen, the overall tendency between the results from Schlünder's formula and the numerical simulations are similar. As shown in the inset in Figure 4, the relative error is greater for this range of very low wetted surface fractions (except, however, for the circular pore when  $\theta < 10^{-5}$ ) compared with the results shown in Figure 3 for greater  $\theta$ . The agreement with the formula for an isolated droplet leads as expected to similar results as Schlünder's formula for sufficiently low  $\theta$  (with the discrepancy due to the numerical prefactor  $2\pi$  versus 4). The comparison with the numerical simulations suggests that Schlünder's formula is more appropriate. However, as shown in Figure 4, the relative error between the numerical simulations and Equation (9) can be relatively high. Further investigations are needed to clarify

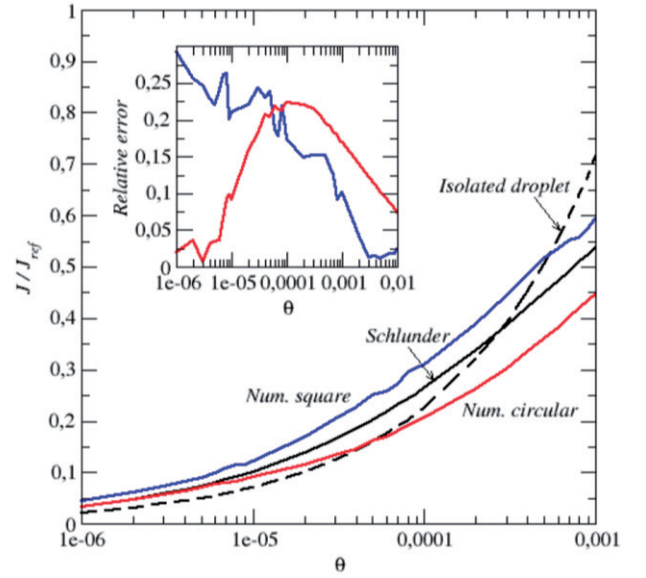


**Figure 4.** Test of Schlünder's relationship in the limit of very low wetted surface fractions as given by Eq. (8). The inset shows the relative error between the numerical results and Schlünder's formula (same color code as for the main plot).

this point, which might be due in part to a combination of numerical inaccuracies owing to the very small region occupied by the wetted surface in the computational domain and the inaccuracy of the Schlünder's formula in the limit of very small  $\theta$ .

Based on the results shown in Figure 4, a very low  $\theta$ , on the order of  $10^{-5}$ , must be considered here to reduce the evaporation rate by a factor 10 compared to the evaporation rate for a fully wet surface. This corresponds to  $r_p/a \approx 1.8 \times 10^{-3}$  (corresponding, for example, to pores of 360 nm in diameter 100  $\mu\text{m}$  away from each other). It can be argued, however, that the boundary layer thickness  $\delta$  is probably affected when the active pores are so sparsely distributed over the surface. Thus, this situation of very low evaporation probably needs further investigation.

### Influence of disorder

Pore sizes are not uniform in a porous medium but vary from one pore to another. Thus, it is interesting to look at the impact of the pore size variability. Here several options are possible. One can play for instance with the distance between two neighbor pores and/or the pore diameters or the pore shapes. Varying the shape, for example, sounds a bit less relevant since the pore shapes should be similar for a given porous medium. So, square pores are considered. For simplicity, we have decided to only vary the pore side length (and thus not the distance between the pore centers). A square arrangement of pore openings at the surface

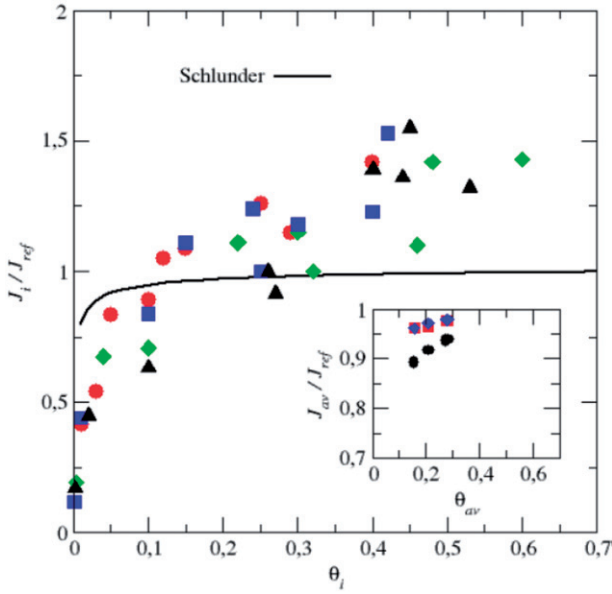


**Figure 5.** Variation of  $J_i/J_{ref}$  with  $\theta_i$  where  $J_{ref}$  is given by Eq. (2),  $\delta = 10$  mm,  $a = 1$  mm. Each type of symbol (filled circles, square, diamond, and triangle) corresponds to one realization of the  $3 \times 3$  surface. The inset shows the variation of the average evaporation rate with average  $\theta$  (black symbols: Schlünder's formula option #1 (i.e., Eq. (1) with Eq. (12)), blue symbols: Schlünder's formula option #2 (i.e., Eq. (1) with Eqs. (13–14)), red symbols: average values from the numerical simulation over the four realizations of the  $3 \times 3$  surface).

is considered for a fixed distance between the centers of two neighbor pores. The pore side lengths are selected randomly as follows. Similarly as in Figure 1(b), a surface with  $3 \times 3$  pore openings is considered (but the openings are square and their sizes vary). First, we select a range of  $\theta$ , namely  $[\theta_{min}, \theta_{max}]$ . Then we select nine values in this range roughly evenly distributed. Then the nine values are randomly located over the nine locations at the surface. The side length  $d$  of each pore is then deduced from the definition of  $\theta$ ,  $\theta = d^2/a^2$ . A surface with nine values of  $\theta$  so distributed is called a realization of the surface. A total of four realizations of the surface are considered in what follows.

The local wetted surface fraction is defined as

$$\theta_i = \frac{d_i^2}{a^2}, \quad (10)$$

where  $i$  is the pore index. Thus  $i$  varies between 1 and 9 since there are 9 pores at the surface.

The global wetted surface fraction is defined as

$$\theta = \frac{\sum_{i=1}^{i=9} d_i^2}{9a^2} = \frac{1}{9} \sum_{i=1}^{i=9} \theta_i. \quad (11)$$

The evaporation rate  $J_i$  from each pore is determined by solving Equations (3–6) for each realization.

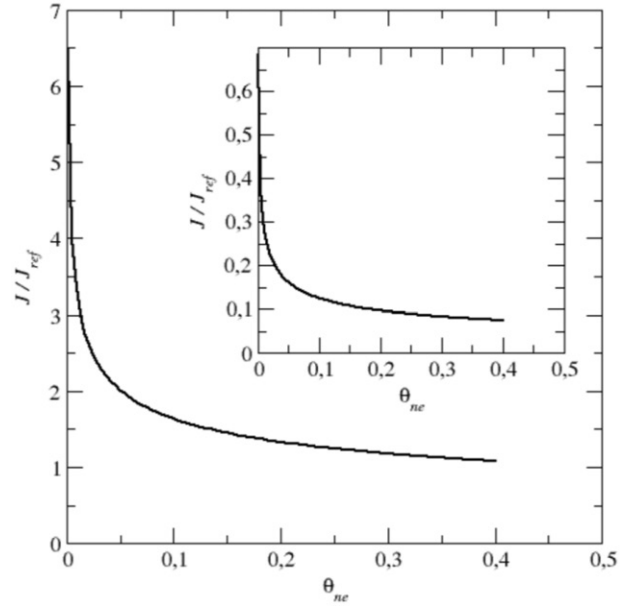


**Figure 6.**  $3 \times 3$  surface with two pore scales. Variation of the evaporation rate from the middle cell for two different wet surface fraction  $\theta_{mi}$  as a function of neighbor cell wet surface fraction  $\theta_{ne}$ . Main plot  $\theta_{mi} = 0.4$ ; inset  $\theta_{mi} = 0.001$ .

Figure 5 shows the variation of  $J_i$  as a function of  $\theta_i$  with a comparison with the predictions using locally the Schlünder's formula (i.e., Equation (1) with  $\theta = \theta_i$ ,  $r_{pi} = d_i/\sqrt{\pi}$ ) for values of  $\theta$  in the range  $[0.001-0.48]$ . As can be seen, using locally Schlünder's formula, that is, for each cell at the surface, leads to poor results. The evaporation rate is underestimated for  $\theta_i$  approximately greater than 0.15 and overestimated for lower  $\theta_i$ .

The variability of the local evaporation rate is quite high (between about 10% of  $J_{ref}$  and 150% of  $J_{ref}$ ). Thus the evaporation rate can be locally 50% greater than the evaporation rate corresponding to a fully wet cell. This is explained by the impact of neighbor pores. It is expected that the evaporation rate from a given pore is greater when the neighbor pores are small on average than when the neighbor pores are greater. This is illustrated in Figure 6 for a special  $3 \times 3$  surface with only two sizes of pore. The pore in the middle of size  $d_{mi}$  (corresponding to  $\theta_{mi}$ ) and the eight neighbor pores of size  $d_{ne}$  (corresponding to  $\theta_{ne}$ ). Figure 6 shows the variation of the evaporation rate from the middle cell for two different wet surface fraction  $\theta_{mi}$  as a function of neighbor cell wet surface fraction  $\theta_{ne}$ . As depicted in Figure 6, the greater are the neighbor pores, the lower the evaporation rate from the middle pores. Also, consistently with the results shown in Figure 5, the dimensionless evaporation rate is greater than one when the middle pore size is greater than the neighbor pore size. Conversely,

the dimensionless evaporation rate is lower than one when the middle pore is smaller than the neighbor pores.

Whereas it is clear from [Figure 5](#) that the simple application of Schlünder's formula to each cell does not lead to good results, one can wonder whether Schlünder's formula can still be used to predict the overall evaporation rate. To this end, two options are considered. Option 1 consists in using the radius corresponding to the whole wet surface area as equivalent pore radius,

$$r_{popt1} = \sqrt{\frac{\sum_{i=1}^{i=9} \theta_i a^2}{\pi}} \quad (12)$$

and for  $\theta$ ,

$$\theta_{popt1} = \frac{\sum_{i=1}^{i=9} \theta_i a^2}{9a^2} = \frac{1}{9} \sum_{i=1}^{i=9} \theta_i. \quad (13)$$

The second option consists in using the average equivalent pore radius, that is

$$r_{popt2} = \frac{1}{9} \sum_{i=1}^{i=9} \sqrt{\frac{\theta_i a^2}{\pi}} \quad (14)$$

with  $\theta_{popt2} = \theta_{popt1}$ . Thus the difference between the two options lies in the definition of the equivalent pore radius. The equivalent pore radius corresponds to the whole wet surface with option 1 and to the average equivalent pore radius with option 2. As can be seen from the inset in [Figure 5](#), option 2 leads to a good agreement with the numerical values. In other terms, replacing the heterogeneous surface by a homogenous surface of nine identical pores having the same size as the average pore size of the heterogeneous surface leads to the same evaporation rate as for the heterogeneous surface.

### Extension of Schlünder's formula to heterogeneous surfaces

Since the size of neighbor pores has an impact, a simple idea is to associate an influence surface  $A_i$  with each pore at the surface. How  $A_i$  can be determined is explained below. Then the evaporation rate from pore  $i$  can be estimated using [Equation \(1\)](#) as

$$\frac{J_i}{J_{refi}} = \frac{1}{1 + \frac{2}{\pi} \frac{r_{pi}}{\delta} \sqrt{\frac{\pi}{4\theta_i}} \left[ \sqrt{\frac{\pi}{4\theta_i}} - 1 \right]} \quad (15)$$

with  $J_{refi} = \frac{M_v}{RT} DA_i \frac{(P_{vs} - P_{v\infty})}{\delta}$ ,  $\theta_i = \frac{d_i^2}{A_i}$ ,  $r_{pi} = \frac{d_i}{\sqrt{\pi}}$ . Under these circumstances, the evaporation rate from pore # $i$  is given by

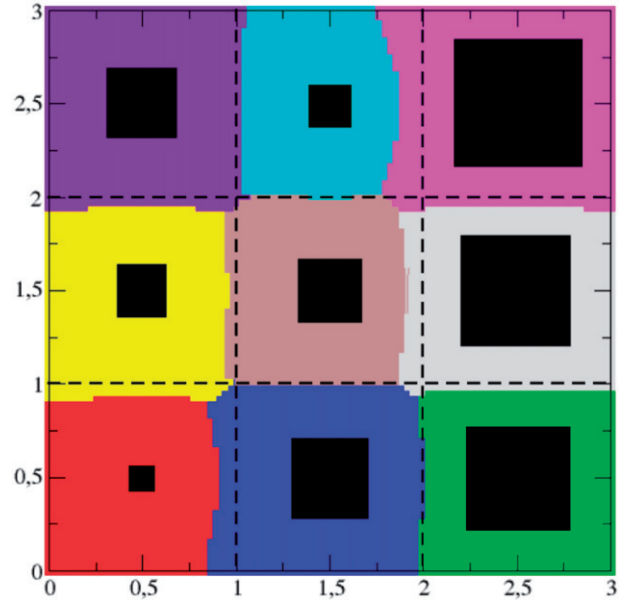


**Figure 7.** Illustration of the influence surfaces (colored areas) associated with each pore (black filled square) at the surface. The dashed lines delineate the boundary of each cell at the surface. The influence surface area of a pore is the surface area of the pore together with the area of the colored surface surrounding the pore. The stairs at the boundary between two influence surfaces are due to the discrete method used to determine the boundary.

$$\frac{J_i}{J_{ref}} = \frac{(A_i/a^2)}{1 + \frac{2}{\pi} \frac{r_{pi}}{\delta} \sqrt{\frac{\pi}{4\theta_i}} \left[ \sqrt{\frac{\pi}{4\theta_i}} - 1 \right]}, \quad (16)$$

where  $a^2$  is the surface area of a cell at the surface and  $J_{ref}$  is given by [Equation \(2\)](#).

In addition to [Equation \(16\)](#), we have also tested a formula in which the impact of the influence surface is taken into account with a power of 2, namely

$$\frac{J_i}{J_{ref}} = \frac{(A_i/a^2)^2}{1 + \frac{2}{\pi} \frac{r_{pi}}{\delta} \sqrt{\frac{\pi}{4\theta_i}} \left[ \sqrt{\frac{\pi}{4\theta_i}} - 1 \right]}. \quad (17)$$

For using [Equations \(16\)](#) or [\(17\)](#), we have to determine the influence surface area  $A_i$  for each pore  $i$ . The idea is simple and consists in making a tessellation of the surface as illustrated for realization #1 in [Figure 7](#).

The influence surface area of a pore is the set of points of the surface which are closer to this pore than to any other pore. To determine the influence surface we use a discrete method based on the pixelization of the surface and determine the number of pixels corresponding to each influence surface. To obtain the tessellation shown in [Figure 7](#), the whole surface was tiled by  $100 \times 100$  square pixels of size  $3a/100$ . It is clear here that more efficient algorithms,

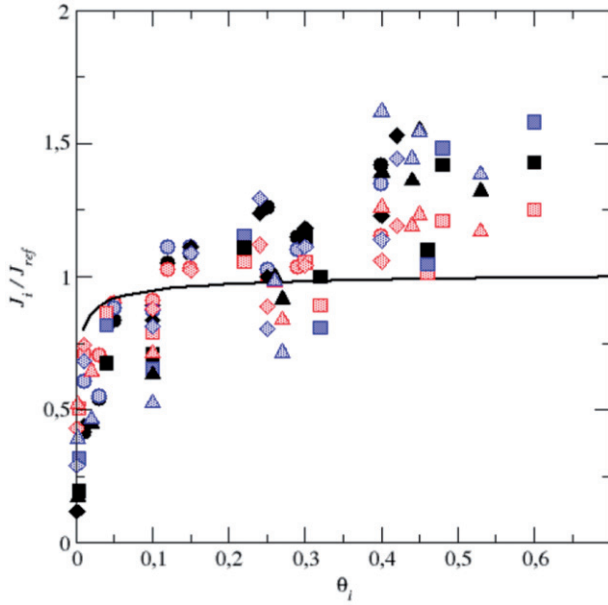


**Figure 8.** Variation of pore evaporation rate  $J_i$  as a function of the corresponding surface cell wetted surface fraction  $\theta_i$  ( $=d_i^2/a^2$ ). The black solid line corresponds to standard Schlünder's formula Eq. (1). The black symbols correspond to the numerical simulations for the four realizations (each type of symbol, circle, square, diamond, triangle, corresponds to one realization). The blue symbols correspond to Eq. (16) and the red ones to Eq. (17).

such as Voronoi tessellation,<sup>[24]</sup> could be used to perform the tessellation. Improving the computational efficiency of the tessellation will be important for extending the method to surface containing a large number of pores.

Application of Equations (16) and (17) then leads to the results shown in Figures 8 and 9.

As can be seen, the use of Equations (16) or (17) significantly improves the prediction from simple formula of Schlünder type. This is better seen in Figure 9, which clearly shows that Equation (17) is the best option. Although the overall trend in Figure 9 is quite good, the scattering for some points in Figure 8 is noticeable.

Also, it can be noted that the discrepancy between the simulations and the prediction from Equation (17) is greater for the smaller pores, which correspond to pores where the evaporation rate rapidly varies with  $\theta_i$ .

### External mass transfer and PNM

As presented for example in Moghaddam et al.<sup>[9]</sup> or Metzger et al.,<sup>[25]</sup> a method for computing the diffusive external mass transfer in the pore network models of drying consists in setting computational nodes in the external layer of size  $\delta$ . However, as illustrated

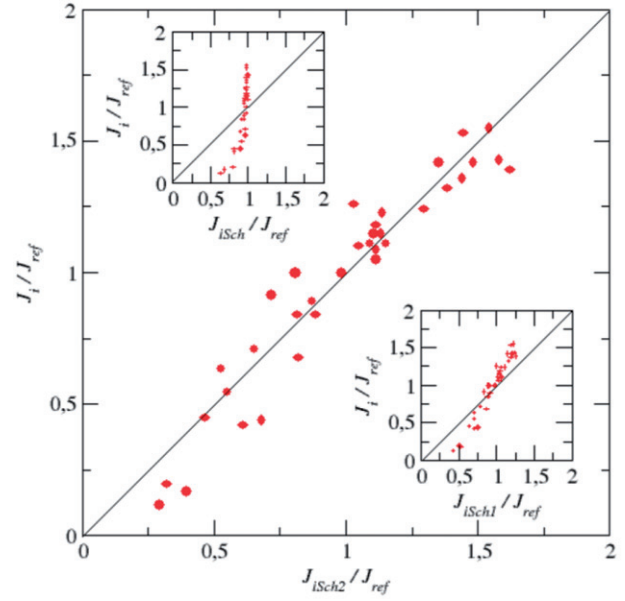


**Figure 9.** Comparison between the evaporation rate from each pore computed numerically and the predictions from the various variants of Schlünder's formula for the  $3 \times 3$  surface. The main plot is the comparison with Eq. (17). The inset on the top left shows the comparison with the standard Schlünder's formula (Eq. (1)). The inset on the bottom right shows the comparison with Eq. (16).

in Figure 10, the distance between two computational nodes is generally taken as the distance between two pores in the network (also referred to as the lattice spacing  $a$ ). Obviously, this is a quite coarse discretization, sufficient to get qualitative results but questionable if the objective is to quantitatively compute the transfer by diffusion in this layer.<sup>[18]</sup> In this context, the objective is to assess the impact of this coarse discretization on the mass transfer at the boundary of the network and also to explore whether the use of Equations (1) or (17) could be a better option.

Consider the case when the pore size does not vary over the surface. Thus, we can consider only a unit cell as depicted in Figure 1(a). The finite volume discretization of the diffusive mass transfer using the coarse discretization classically used in PNM leads to compute the evaporation rate as (see Appendix)

$$\frac{J_{\text{PNM}}}{J_{\text{ref}}} = \frac{2\theta n}{2\theta(n-0.5) + 1}, \quad (18)$$

where  $n = \delta/a$  is the number of finite volumes used in the vertical direction to discretize the boundary layer. A comparison between the results obtained from Equation (18) and from Schlünder's formula (Equation (1)) is presented in Figure 11 considering again the representative values  $\delta = 1$  mm,  $a = 0.1$  mm.

We know from previous sections that Schlünder's formula leads to quite accurate results for this case.

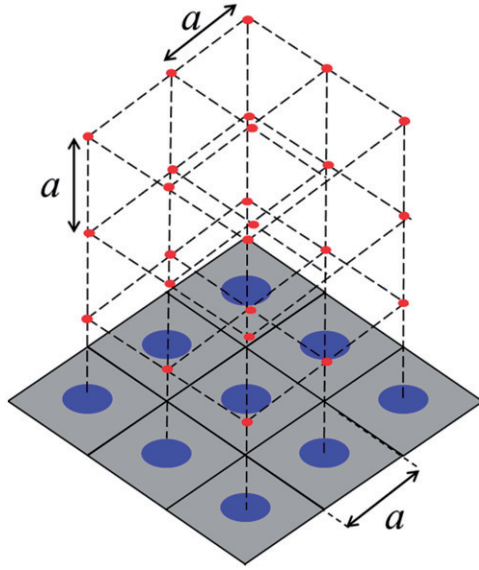


**Figure 10.** Typical distribution of computational nodes (red dots) in the external diffusive mass boundary layer in PNM of drying.

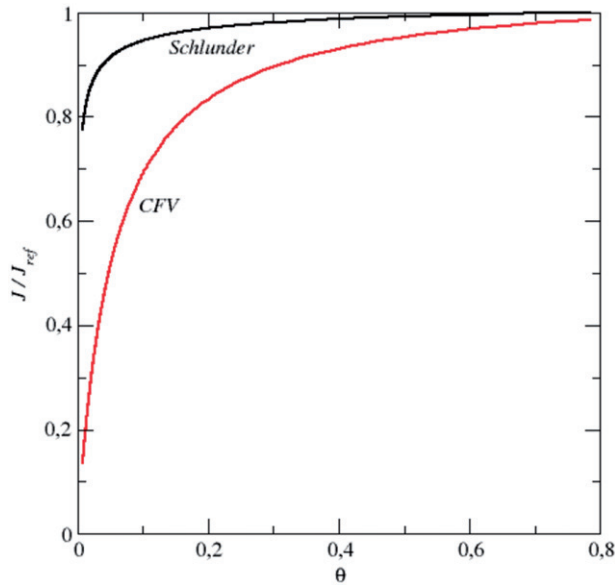


**Figure 11.** Comparison between the results from a coarse finite volume discretization (CFV, Eq. (18)) and from Schlünder's formula (Eq. (1)).  $\delta = 1$  mm,  $a = 0.1$  mm.

Thus, it is clear from the comparison shown in Figure 11 that the coarse discretization used in several previous works with PNM is not satisfactory. A finer discretization is necessary for accurate results. Based on the above, a simpler and better option would be to use the modified Schlünder's formula, that is, Equation (17), as boundary condition for each cell at the evaporative surface instead of the coarse discretization. This approach does not require setting computational points in the boundary layer and therefore

is more computationally efficient than the usual coarse discretization method. It only needs a pre-processing step for determining the influence surface area of each pore at the surface.

## Summary and discussion

The modeling of drying implies to couple the external and internal transfers. The full coupled approach implies to solve the governing equations also in the external gas. This is computationally time consuming. Developing simplified approaches is therefore highly desirable. In fact, this problem is usually circumvented by the use of a mass transfer coefficient at the surface. This is not satisfactory in general because the spatial and temporal variations of this coefficient are generally not known a priori. Actually, this type of coefficient is rather used as a fitting parameter. This can be useful in practice but not satisfactory from a modeling/theoretical standpoint. In this context, Equation (1) provides a simple relationship to determine the evaporation rate from a partially wet surface when the external transfer is dominated by diffusion.

In this work, we have explored the value of Schlünder's formula, that is, Equation (1), as a possible relationship for computing the evaporation rate from the individual pores of a model porous surface. When the surface is spatially periodic with a uniform pore size, Schlünder's formula provides a quite reasonable estimate of the evaporation rate. However, the quality of the prediction depends on the pore shape, that is, on how the wet fraction is distributed over the surface cells. Also, the estimate is less good for very small wet surface fractions.

The consideration of heterogeneous surfaces characterized by a spatial variability in the pore size leads to interesting results, especially in relation with the PNM of drying. The standard application of Schlünder's formula leads to poor results. The evaporation rate from the bigger pores is significantly underestimated whereas the evaporation rate from the smaller pores is significantly overestimated. This is a consequence of the surface heterogeneity. The evaporation rate from a cell depends on the size of neighbor pores. It is greater when the neighbor pores are smaller and lower when they are larger than the pore of the considered cell.

These results led to introduce the concept of pore influence surface in order to take into account the pore size heterogeneity while still using Schlünder's formula.

The influence surface of a pore was defined as the set of the points of the surface closer to this pore than

to any other pores. This leads to the tessellation of the whole surface by the influence surfaces and results in a greater influence surface for a larger pore than for a smaller pore. Using the influence surfaces with Schlünder's formula greatly improves the comparison between the analytical prediction of the evaporation rate from each pore at the surface and the evaporation rate obtained from numerical simulations. Yet, this was obtained by using a correction factor involving the ratio of the influence surface to the cell surface with an exponent equal to 2. Why this value of the exponent leads to better results than an exponent equal to 1 remains to be justified from a theoretical standpoint.

The use of Schlünder's formula with the influence surfaces provides a simple mean to impose the boundary condition at the surface in the PNM of drying when the external transfer is controlled by diffusion over a layer of given thickness. The relatively classical method consisting in computing the transfer in the diffusive layer with a coarse discretization using a discretization step equal to the spacing of the underlying lattice is clearly just a quite crude and inaccurate method. For accurate computations, a much finer discretization is mandatory. In order to avoid the corresponding high computational cost, it is thus recommended to use Schlünder's formula with the influence surface, that is, Equation (17). Although less accurate than a refined computation, this approach is much better than the classical approach using the lattice spacing as discretization step.

However, it should be recalled that this method has only been tested over a small surface with only nine pores and only four realizations. More work is needed to confirm the general validity of the method. Basically, surfaces with more pores, as well as other types of surfaces, for instance surfaces where both the distance between two neighbor pores and the pore size vary, must be tested.

Also, we have considered a surface where the vapor concentration is the same at the surface of each pore. As illustrated for instance in Moghaddam et al.<sup>[9]</sup> from pore network simulations, the vapor concentration at the surface pore entrances actually varies during drying because of the invasion of an increasing fraction of pores by the gas phase. Both the wet pores and the dry pores at the surface contribute to the evaporation rate since vapor transport can also occur through the dry pores. Thus, the impact of the vapor concentration variability on the results obtained from Schlünder's formula with the influence surfaces must be also assessed.

## Funding

Financial support from joint project "Drycap" funded by GIP ANR (project16-CE92-0030-01) and DFG (project TS28/10-1) is gratefully acknowledged.

## References

- [1] Lenormand, R.; Touboul, E.; Zarcone, C. Numerical Models and Experiments on Immiscible Displacements in Porous Media. *J. Fluid Mech.* **1988**, *189*, 165–187.
- [2] Shaw, T. M. Drying as an Immiscible Displacement Process with Fluid Counterflow. *Phys. Rev. Lett.* **1987**, *59*, 1671–1674.
- [3] Tsimpanogiannis, I. N.; Yortsos, Y.; Poulou, S.; Kanellopoulos, N.; Stubos, A. K. Scaling Theory of Drying in Porous Media. *Phys. Rev. E.* **1999**, *59*, 4353–4365.
- [4] Prat, M.; Bouleux, F. Drying of Capillary Porous Media with a Stabilized Front in Two Dimensions. *Phys. Rev. E. Stat. Phys. Plasmas. Fluids. Relat. Interdiscip. Topics.* **1999**, *60*, 5647–5656.
- [5] Schlünder, E. U. On the Mechanism of the Constant Drying Rate Period and Its Relevance to Diffusion Controlled Catalytic Gas Phase Reactions. *Chem. Eng. Sci.* **1988**, *43*, 2685–2688.
- [6] Shahraeeni, E.; Lehmann, P.; Or, D. Coupling of Evaporative Fluxes from Drying Porous Surfaces with Air Boundary Layer: Characteristics of Evaporation from Discrete Pores. *Water Resour. Res.* **2012**, *48*, W09525.
- [7] Suzuki, M.; Maeda, S. On the Mechanism of Drying of Granular Beds. *J. Chem. Eng. Jpn.* **1968**, *1*, 26–31.
- [8] Haghghi, E.; Shahraeeni, E.; Lehmann, P.; Or, D. Evaporation Rates Across a Convective Air Boundary Layer Are Dominated by Diffusion. *Water Resour. Res.* **2013**, *49*, 1602–1610.
- [9] Moghaddam, A. A.; Kharaghani, A.; Tsotsas, E.; Prat M. A Pore Network Study of Evaporation from the Surface of a Drying Non-Hygroscopic Porous Medium. *AIChE J.* **2018**, *64*, 1435–1447.
- [10] Lehmann, P.; Or, D. Effect of Wetness Patchiness on Evaporation Dynamics from Drying Porous Surfaces. *Water Resour. Res.* **2013**, *49*, 8250–8262.
- [11] Schlünder, E. U. Drying of Porous Material During the Constant and the Falling Rate Period: A Critical Review of Existing Hypotheses. *Drying Technol.* **2004**, *22*, 1517–1532.
- [12] Chen, P.; Pei, D. C. T. A Mathematical Model of Drying Processes. *Int J. Heat Mass Transfer.* **1989**, *32*, 297–310.
- [13] Masmoudi, W.; Prat, M. Heat and Mass Transfer Between a Porous Medium and a Parallel External Flow, Application to Drying of Capillary Porous Materials. *Int. J. Heat Mass Trans.* **1991**, *34*, 1975–1989.
- [14] Erriguible, A.; Bernada, P.; Couture, F.; Roques, M. A. Modeling of Heat and Mass Transfer at the Boundary Between a Porous Medium and Its Surroundings. *Drying Technol.* **2005**, *23*, 455–472.

- [15] Defraeye, T.; Blocken, B.; Derome, D.; Nicolai, B.; Carmeliet, J. Convective Heat and Mass Transfer Modelling at Air–Porous Material Interfaces: Overview of Existing Methods and Relevance. *Chem. Eng. Sci.* **2012**, *74*, 49–58.
- [16] Jambhekar, V. A.; Helmig, R.; Schröder, N.; Shokri, N. Free-Flow-Porous-Media Coupling for Evaporation-Driven Transport and Precipitation of Salt. *Transp. Porous Med.* **2015**, *110*, 251–280.
- [17] Masson, R.; Trenty, L.; Zhang, Y. Coupling Compositional Liquid Gas Darcy and Free Gas Flows at Porous and Free-Flow Domains Interface. *J. Comput. Phys.* **2016**, *321*, 708–728.
- [18] Xu, Z.; Pillai, K. M. Analyzing Slow Drying in a Porous Medium Placed Adjacent to Laminar Airflow Using a Pore-Network Model. *Numer. Heat Transf., Part A Appl.* **2016**, *70*, 1213–1231.
- [19] Veran-Tissoires, S.; Prat, M. Evaporation of a Sodium Chloride Solution from a Saturated Porous Medium with Efflorescence Formation. *J. Fluid Mech.* **2014**, *749*, 701–749.
- [20] Yiotis, A. G.; Tsimpanogiannis, I. N.; Stubos, A. K.; Yortsos, Y. Pore-Network Study of the Characteristic Periods in the Drying of Porous Materials. *J. Colloid Interface Sci.* **2006**, *297*, 738–748.
- [21] Eloukabi, H.; Sghaier, N.; Ben Nasrallah, S.; Prat, M. Experimental Study of the Effect of Sodium Chloride on Drying of Porous Media: The Crusty-Patchy Efflorescence Transition. *Int. J. Heat Mass Tr.* **2013**, *56*, 80–93.
- [22] Picknett, R. G.; Bexon, R. The Evaporation of Sessile or Pendant Drops in Still Air. *J. Colloid Interface Sci.* **1977**, *61*, 336–350.
- [23] Hu, H.; Larson, R. G. Evaporation of a Sessile Droplet on a Substrate. *J. Phys. Chem. B.* **2002**, *106*, 1334–1344.
- [24] Atsuyuki, O.; Boots, B.; Sugihara, K.; Chiu, S. N. *Spatial Tessellations: Concepts and Applications of Voronoi Diagrams*; 2nd ed. John Wiley & Sons: Chichester, **1999**.
- [25] Metzger, T.; Tsotsas, E.; Prat, M. Pore Network Models: A Powerful Tool to Study Drying at the Pore Level and Understand the Influence of Structure on Drying Kinetics, In *Modern Drying Technology, Computational Tools at Different Scales*, Vol. 1, Mujumdar, A., and Tsotsas, E.; Wiley: Brisbane, **2007**; pp 57–102.
- [26] Laurindo, J. B.; Prat, M. Numerical and Experimental Network Study of Evaporation in Capillary Porous Media. Drying Rates. *Chem. Eng. Sci.* **1998**, *53*, 2257–2269.

## Appendix

### Derivation of Equation (18)

Although the derivation is performed for the 3D case, consider for simplicity the 2D mesh illustrated in Figure A1 (viewed as a cross-section of the 3D mesh).

The finite volume discretization of the diffusion equation over this mesh leads to

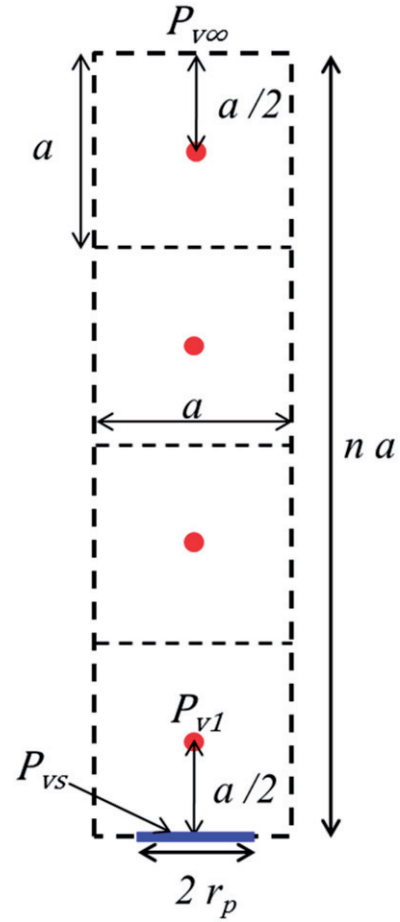


**Figure A1.** Finite volume distribution in the external diffusive mass boundary layer used to obtain Eq. (A-5). The thick blue line materializes the wet pore at the surface. The red dots correspond to the computational points.

$$\pi r_p^2 \left( \frac{P_{v1} - P_{vs}}{a/2} \right) + a^2 \left( \frac{P_{v1} - P_{v\infty}}{(n - 0.5)a} \right) = 0. \quad (\text{A-1})$$

Equation (A-1) can be expressed as

$$2\theta(n - 0.5)(P_{v1} - P_{vs}) + (P_{v1} - P_{v\infty}) = 0. \quad (\text{A-2})$$

The evaporation rate is expressed as

$$J = \frac{M_v}{RT} D \pi r_p^2 \frac{(P_{vs} - P_{v1})}{a/2}. \quad (\text{A-3})$$

Combining Equations (A-3) and (A-2) leads to

$$J = \frac{M_v}{RT} D \frac{2\pi r_p^2}{a} \frac{(P_{vs} - P_{v\infty})}{2\theta(n - 0.5) + 1}. \quad (\text{A-4})$$

Then using Equation (2) leads to express  $J_{\text{ref}}$  here as  $J_{\text{ref}} = \frac{M_v}{RT} Da^2 \frac{(P_{vs} - P_{v\infty})}{na}$ . Combining the latter relationship with Equation (A-4) yields

$$\frac{J}{J_{\text{ref}}} = \frac{2\theta n}{2\theta(n - 0.5) + 1}, \quad (\text{A-5})$$

which is Equation (18) in the main text.

The mesh illustrated in Figure A1 is representative of the mesh used for instance in Laurindo and Prat.<sup>[26]</sup> In other

works on drying using PNM, slightly different discretization choices could have been done but most of them use the same discretization step in the external mass transfer layer as in the PNM. Thus, the significant discrepancies between

Equations (1) and (18) in Figure 11 are representative of the coarse discretization used in the external mass transfer layer and should be similar whatever the details of the finite difference or finite volume formulation.